Electronic Supplementary Material (ESI) for Dalton Transactions.
This journal is © The Royal Society of Chemistry 2018

Supporting Information for

Pseudotetrahedral Cobalt(II) Complexes with PNP-Ligand Showing Uniaxial Magnetic Anisotropy

Yuan-Qi Zhai, [a] Yi-Fei Deng, [a] and Yan-Zhen Zheng*, [a]

[a] Frontier Institute of Science and Technology (FIST), State Key Laboratory for Mechanical Behavior of Materials, MOE Key Laboratory for Nonequilibrium Synthesis of Condensed Matter and School of Science, Xi'an Jiaotong University, 99 Yanxiang Road, Xi'an, Shaanxi 710054, P. R. China.

Email: zheng.yanzhen@xjtu.edu.cn (Y. Z. Z.)

Table of contents

1. General Experimental Section

All reagents were purchased from commercial suppliers and used as received unless stated otherwise. All the solvents were dehydrated and deoxygenated by using solvent purification systems prior to use. All manipulations were performed under a dry and oxygen-free argon atmosphere in a glovebox. The PNP ligand has been synthesized according to the published procedures.[1]

Syntheses of $Co(PNP)Cl_2$ (1)

PNP (283 mg, 0.5 mmol), $CoCl_2$ (63 mg, 0.5 mmol), THF (5 mL) were mixed and transferred into a conical flask (25 mL), then stirred at room temperature for 12 hours. After stirring, the resulting products were dissolved in CH_2Cl_2 and put into a test tube for volatilization, and green block crystals of **1** were obtained in yields of 72% (based on Co, 250 mg). Anal. Calcd (%) for **1**: C, 65.63; H, 4.78; N, 2.01. Found: C, 66.29; H, 5.21; N, 1.98.

Syntheses of $Co(PNP)(SCN)_2$ (2)

A mixture of PNP (283 mg, 0.5 mmol), $Co(SCN)_2$ (87.5 mg, 0.5 mmol) and THF (5 mL) were added into a conical flask (25 mL), then stirred at room temperature for 12 hours. After stirring, the sediment were dissolved in CH_2Cl_2 and put into a test tube for slow evaporation, and green block crystals of **2** were obtained in yields of 51% (based on Co, 188 mg). Anal. Calcd (%) for **2**: C, 64.86; H, 4.49; N, 5.67. Found: C, 65.25; H, 4.76; N, 5.43.

2. X-Ray Crystallography Data

Single crystals suitable for X-ray analysis were coated with deoxygenated Paratone-N oil. All data were collected on a Bruker Apex II DUO area-detector diffractometer with graphite-monochromatic Mo Kα radiation (λ = 0.71073 Å). Cell refinement and data reduction were accomplished with the SAINT processing program. The structures were solved by direct methods and refined on F^2 using SHELXTL [2].

Table S1. X-ray crystallographic data for complexes **1** and **2**.

	1	**2**
formula	$C_{38}H_{33}CoNP_2Cl_2$	$C_{40}H_{33}CoN_3P_2S_2$
M/g mol^{-1}	695.42	740.68
crystal system	Orthorhombic	Monoclinic
space group	$Pna2_1$	$P2_1/c$
a, Å	17.191(4)	10.221(2)
b, Å	10.438(3)	18.725(4)
c, Å	19.367(4)	21.287(4)
α, deg	90	90
β, deg	90	114.070(8)
γ, deg	90	90
V, Å^3	3475.2(15)	3719.8(13)
Z	4	4
d_{cal}/g cm^{-1}	1.329	1.323
temperature, K	296(2)	296(2)
θ range	2.10 – 27.53°	1.51 – 27.67°
completeness	0.992	0.992
Goodness-of-fit on F^2	1.154	1.004
final indices [$I > 2\sigma(I)$]	R_1 = 0.0439, wR_2 = 0.0483	R_1 = 0.0464, wR_2 = 0.1006
R indices (all data)	R_1 = 0.0820, wR_2 = 0.0534	R_1 = 0.0904, wR_2 = 0.1175

Table S2. Selected bond lengths (Å) and angles (°) for complex **1**.

Bonds	Å	Angel	°
Co(1) – P(1)	2.399(1)	Cl(1) – Co(1) – Cl(2)	109.41(5)
Co(1) – P(2)	2.376(1)	Cl(1) – Co(1) – P(2)	103.76(4)
Co(1) – Cl(1)	2.236(9)	Cl(1) – Co(1) – P(1)	107.09(4)
Co(1) – Cl(2)	2.242(1)	Cl(2) – Co(1) – P(2)	110.32(4)
		Cl(2) – Co(1) – P(1)	115.97(3)
		P(1) – Co(1) – P(2)	109.54(4)

Table S3. Selected bond lengths (Å) and angles (°) for complex **2**.

Bonds	Å	Angel	°
Co(1) - P(1)	2.362(9)	N(2) – Co(1) – N(3)	108.34(11)
Co(1) - P(2)	2.377(9)	N(2) – Co(1) – P(1)	108.33(9)
Co(1) - N(2)	1.931(3)	N(2) – Co(1) – P(2)	107.49(8)
Co(1) - N(3)	1.938(3)	N(3) – Co(1) – P(1)	110.01(8)
		N(3) – Co(1) – P(2)	111.00(8)
		P(1) – Co(1) – P(2)	111.55(3)

Table S4. The best results fitted for **2** under 3000 Oe dc field by a generalized Debye model.

T / K	τ/s	α
1.8	9.50×10^{-4}	0.22
1.9	7.59×10^{-4}	0.19
2.0	5.79×10^{-4}	0.14
2.1	4.01×10^{-4}	0.09
2.2	2.66×10^{-4}	0.07
2.3	1.79×10^{-4}	0.06
2.4	1.10×10^{-4}	0.06
2.5	5.61×10^{-5}	0.06

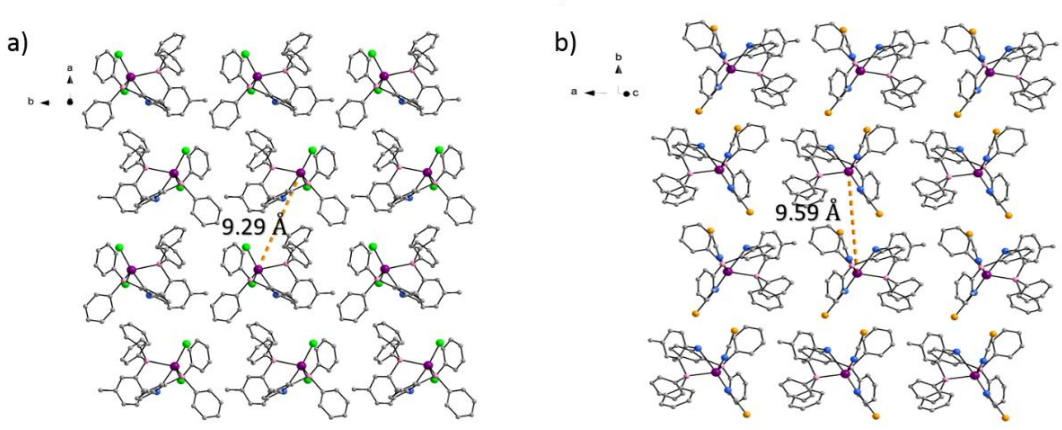

Figure S1. Packing arrangement of **1** (a) and **2** (b). The dashed line shows the nearest intermolecular Co···Co separation (Å). Hydrogen atoms are omitted for clarity. Colour codes: Co, purple; S, yellow; P, lavendar; C, grey; N, blue; Cl, light green.

3. Powder X-ray Diffraction

The X-ray powder diffraction (PXRD) measurements for complexes **1** and **2** were performed on a Rigaku SmartLab X-ray diffractometer at room temperature, which was in good agreement with the simulations from the single crystal data, indicating the high purity of the samples.

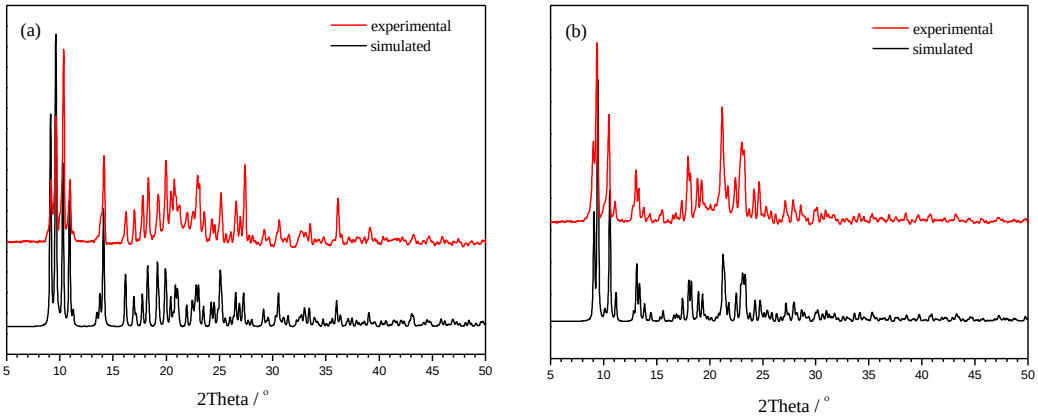

Figure S2. The powder X-ray diffractions for **1** (a) and **2** (b). The black curve is calculated from the single crystal data.

4. FT-IR Spectra

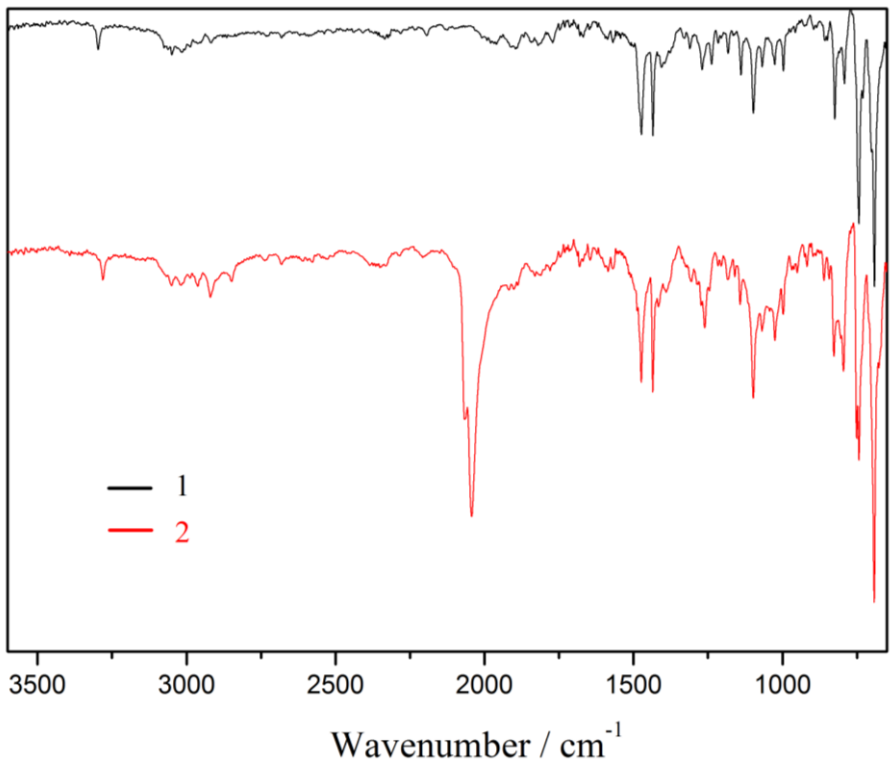

Figure S3. IR spectra of indicated complexes.

5. Magnetic Data

Magnetic measurements were performed on polycrystalline samples sealed in polyethylene film. Data were collected using a Quantum Design MPMS-XL7 SQUID magnetometer from 2.0 to 300 K at applied dc fields ranging from 0 to +7 T. Dc susceptibility data were corrected for diamagnetic contributions from the sample holder and for the core diamagnetism of each sample estimated using Pascal's constants. Ac magnetic susceptibility data for **2** were collected under a dc field of 3000 Oe and an ac field of 3.5 Oe, oscillating at frequencies in the range of 1 – 1500 Hz. Frequency-dependent ac susceptibility data were used to construct Cole–Cole plots, which were then fitted using a generalized Debye model to estimate relaxation times.

In PHI program, we first set the spin S = 3/2 and the orbital moment L = 0 for the central Co(II) ion, namely the normal set for a Co(II) ion in a T_d symmetry. Then we used an initial guess with D = -10 cm^{-1}, E = 0, g_{iso} = 2 and TIP = 0 (This can be set to any value) and run the program to yield a best fit of the dc magnetic spectra. Finally the parameters of the fitting were got with high accuracy.

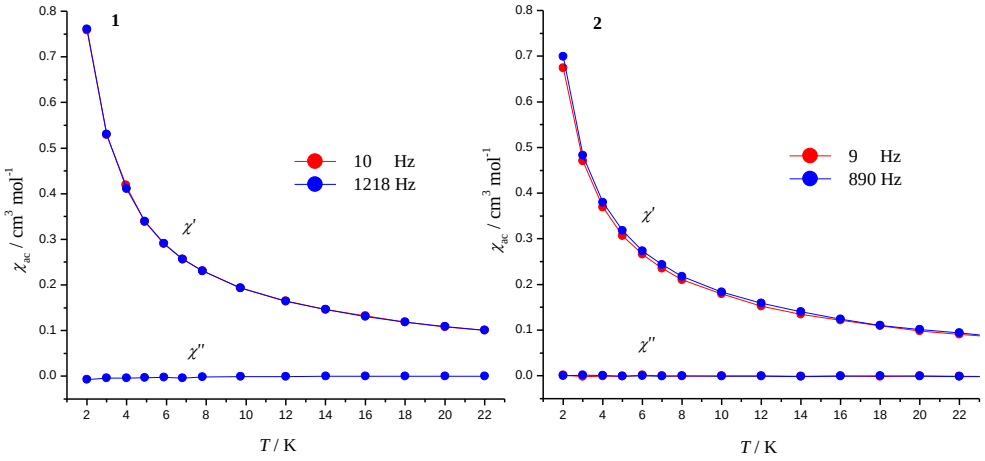

Figure S4. Temperature dependence of the in-phase (χ') and out-of-phase (χ'') ac susceptibility for **1** and **2** under zero dc field. The lines are guides to the eyes.

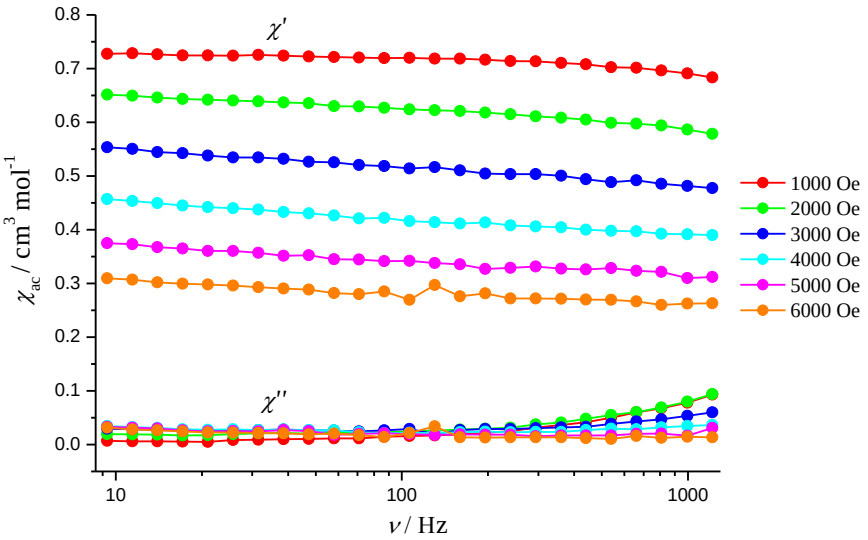

Figure S5. Frequency dependence of the in-phase (χ') and out-of-phase (χ'') ac susceptibility for **1** at 2 K under different dc fields. The lines are guides to the eyes.

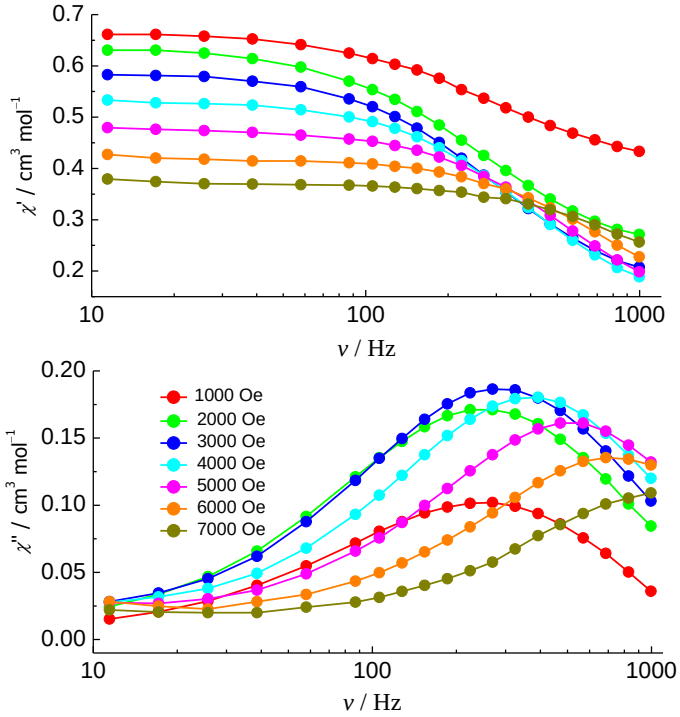

Figure S6. Frequency dependence of the in-phase (χ') and out-of-phase (χ'') ac susceptibility for **2** at 2 K under different dc fields. The lines are guides to the eyes.

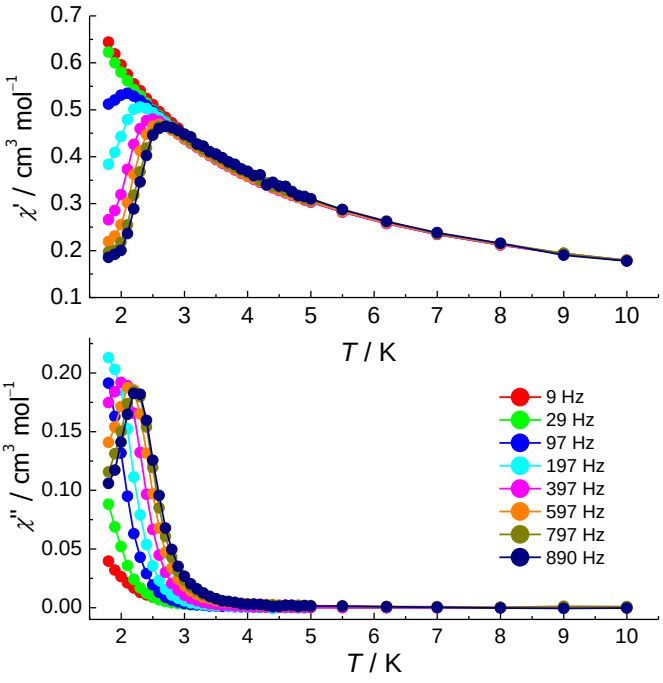

Figure S7. Temperature dependence of the in-phase (χ') and out-of-phase (χ'') ac susceptibility for **2** under 3000 Oe dc field. The lines are guides to the eyes.

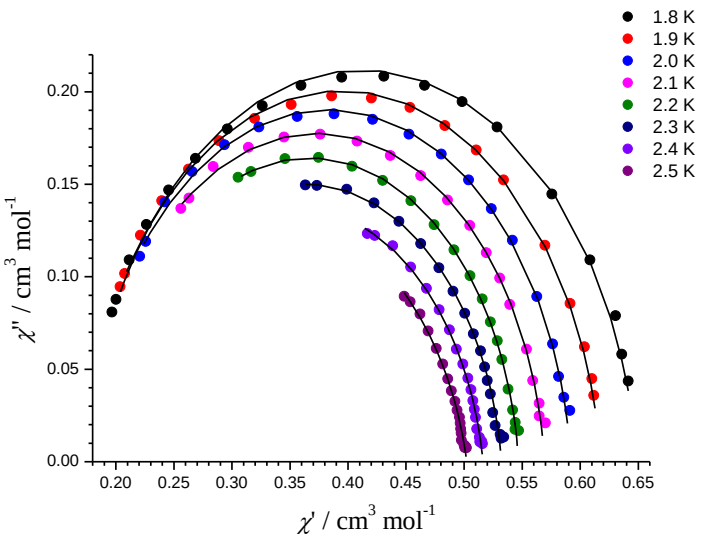

Figure S8. Cole-Cole plots for **2** at 3000 Oe dc field. The solid lines represent the best fit to the data.

6. HF-EPR Measurements

HF-EPR measurements were performed on a locally developed spectrometer at Wuhan National High Magnetic Field Centre, using a pulsed magnetic field of up to 30 T in a frequency range from 60GHz to 505GHz. [3] The single-frequency spectra were simulated and spin Hamiltonian parameters were fitted using SPIN program developed by Andrew Ozarowski in the National High Magnetic Field Laboratory, USA.

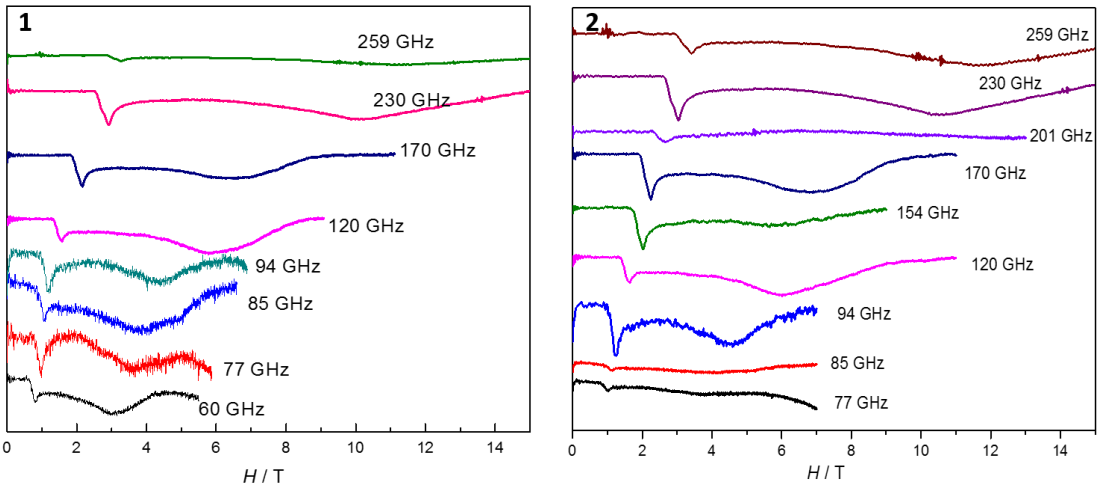

Figure S9. Variable-frequency EPR spectra collected on a powder sample of **1** and **2** at 4.2 K.

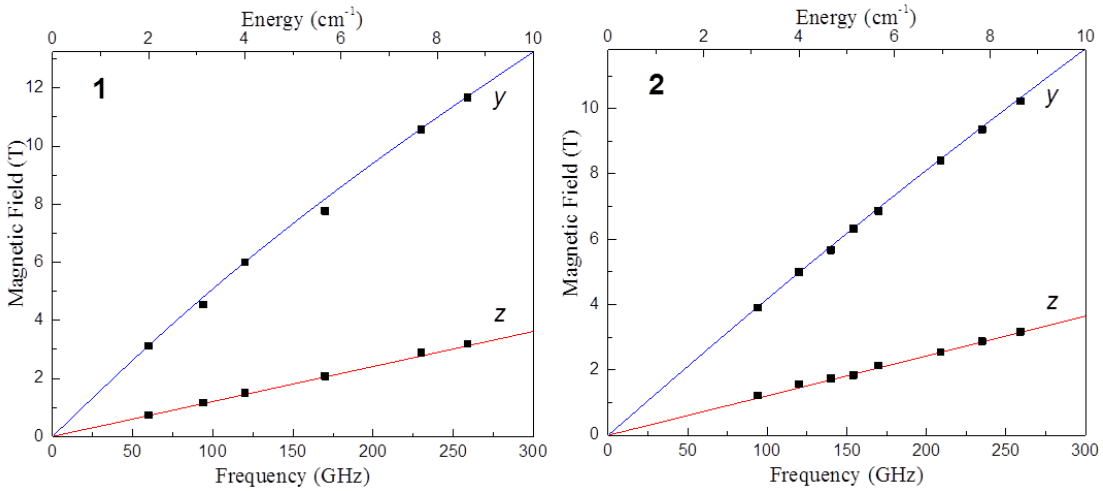

Figure S10. 2D field/frequency maps of EPR transitions for **1** and **2** at 4.2 K. Solid lines are the (y, z) transitions.

7. Theoretical Calculations

Ab initio multiconfigurational calculations were performed using the ORCA 4.0 computational package [4]. The polarized triple-ζ-quality basis set [def2-TZVP] proposed by Ahlrichs and co-workers was used for cobalt and coordinated nitrogen atoms, while the basis set def2-SVP was used for other remote atoms.[5] Meanwhile, the scalar relativistic effects were taken into account with a standard second-order Douglas-Kroll-Hess (DKH2)[6] for heavy ion cobalt(II) and the auxiliary basis set def2/J was used in conjunction with the resolution of identity approximation. The state-average (SA)-CASSCF[7a] calculations, followed by N-electron valence perturbation theory to second order (NEVPT2)[7b – 7e] step to account for the major part of the differential dynamic correlation between the ground and the excited states, was composed of 7 metal 3d electrons and 5 3d orbitals [CAS(7,5)], with 10 states for quartet states and 40 states for doublet states, which has been used by many works[8].

From a theoretical prospect, the so-called spin Hamiltonian is generally a model Hamiltonian[9a]. However, the spin-orbit coupling (SOC) of Co^{2+} is too strong to use the so-called spin-free Hamiltonian[9b-9d], so that we used the Breit-Pauli approximation to introduce the SOC Hamiltonian containing one- and two- electron parts:

$$\hat{H}_{SO} = \frac{\alpha^2}{2}\sum_A\sum_i \frac{Z_A}{|\vec{R}_A-\vec{r}_i|^3}\hat{\vec{l}}_i^{\,A}\hat{\vec{s}}_i - \frac{\alpha^2}{2}\sum_i \hat{\vec{s}}_i \sum_{j\neq i}\frac{1}{|\vec{r}_i-\vec{r}_j|^3}(\hat{\vec{l}}_i^{\,j} + 2\hat{\vec{l}}_j^{\,i}) \qquad (1)$$

where α is the fine structure constant, $\hat{\vec{l}}_i^{\,A} = (\vec{r}_i - \vec{R}_A)\times\vec{p}_i$ stands for the angular momentum of the i-th electron relative to nucleus *A* with charge Z_A at the position $\vec{R}_A$, and $\hat{\vec{l}}_i^{\,j} = (\vec{r}_i - \vec{R}_j)\times\vec{p}_i$ is the angular momentum of the electron i relative to electron j. To compute one- and two- parts of the SOC Hamiltonian both, we used the mean field approximation (SOMF)[10] where the overall Hamiltonian can be written as

$$\hat{H}_{SO} = \sum_A\sum_i \xi(r_{iA})\hat{\vec{l}}_i^{\,A}\hat{\vec{s}}_i \qquad (2)$$

where $\xi(r_{iA}) = \frac{\alpha^2}{2}\frac{Z_{A\,eff}}{|\vec{R}_A-\vec{r}_i|^3}$ is the effective function of SOC effect of electron I relative to the nucleus A and parameters $Z_{A\,eff}$ are chosen empirically.

Then the spin Hamiltonian can be written as

$$\hat{H}_{eff} = \hat{H}_{BO} + \hat{H}_{SO} + \hat{H}_S \quad (3)$$

where $\hat{H}_{BO} = -\sum_{i=1}^{N} \frac{1}{2}\nabla_i^2 - \sum_{i=1}^{N}\sum_{i=1}^{M} \frac{Z_A}{|r_i - R_A|} + \frac{1}{2}\sum_{i\neq j=1}^{N} \frac{1}{|r_i - r_j|} + \frac{1}{2}\sum_{A\neq B=1}^{M} \frac{Z_A Z_B}{|R_A - R_B|}$ is the Born-Oppenheimer Hamiltonian and $\hat{H}_s = \hat{S}D\hat{S} + \mu_B B g \hat{S}$ is the spin-free Hamiltonian. *D* and *g*, represent the zero-field splitting and anisotropic Zeeman interaction of the paramagnetic ion, respectively. The effective Hamiltonian approach (EHA)[11] was used to extract spin Hamiltonian parameters from ab initio results as have been proven to be appropriate. Therefore, the spin Hamiltonian parameters, namely *D*, *E* and *g* tensors, were calculated. Meanwhile, tight SCF convergence criteria was used to maintain the calculation accuracy.

Table S5. The relative energies of ground and low-lying quartet spin eigenstates (cm^{-1})

	1	**2**
$^4\Psi_0$	0.0	0.0
$^4\Psi_1$	4312.9	5186.5
$^4\Psi_2$	4880.3	6197.4
$^4\Psi_3$	5646.8	6248.5
$^4\Psi_4$	7403.6	9381.2
$^4\Psi_5$	8729.7	9537.9
$^4\Psi_6$	11233.0	12049.5
$^4\Psi_7$	18617.7	19213.4
$^4\Psi_8$	20674.2	21508.3
$^4\Psi_9$	22135.9	23718.4

Table S6. The relative energies of ground and first excited Kramers doublets (KD) (cm^{-1}) and their Boltzmann populations at *T* = 300 K.

	KD		Boltzmann populations
1	KD_0	0.0	0.263
	KD_1	22.4	0.237
	KD_2	4288.2	3.08e-10
2	KD_0	0.0	0.261
	KD_1	19.1	0.239
	KD_2	5192.8	4.00e-12

Table S7. The relative energies of d-orbitals for **1** and **2** (cm^{-1}).

	1	**2**
d_{z2}	0.0	0.0
d_{x2-y2}	583.3	328.6
d_{yz}	3791.5	4022.3
d_{xz}	4497.3	4840.6
d_{xy}	5394.3	6517.0

Table S8. Individual contribution to *D*-tensor calculated by CASSCF/NEVPT2 (cm^{-1}).

Multiplicity	Root	**1**	**2**
4	1	-19.1	-16.3
	2	7.9	5.1
	3	2.7	2.6
	4	-1.2	/
2	6	1.9	1.7
	7	-2.5	-3.2

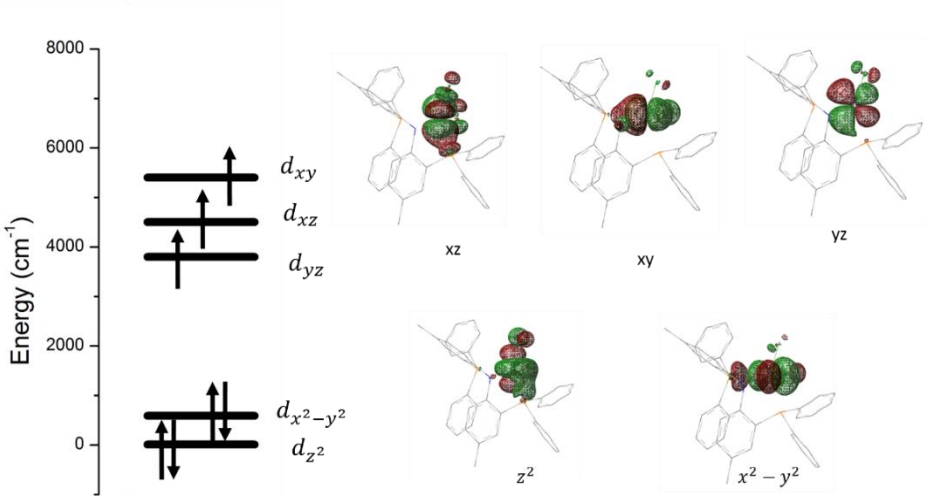

Figure S11. NEVPT2 computed active orbital energy orderings for lowest-lying quartet state for **1**.

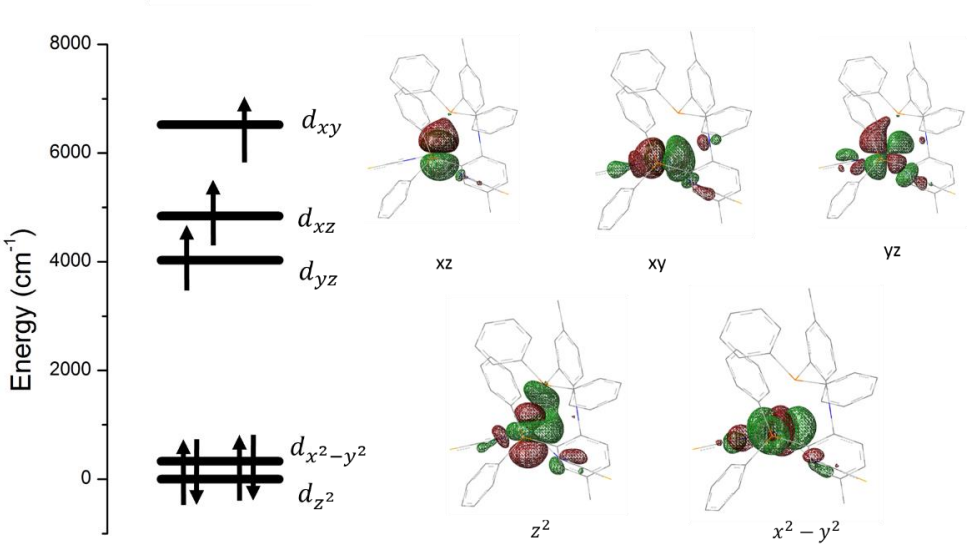

Figure S12. NEVPT2 computed active orbital energy orderings for lowest-lying quartet state for **2**.

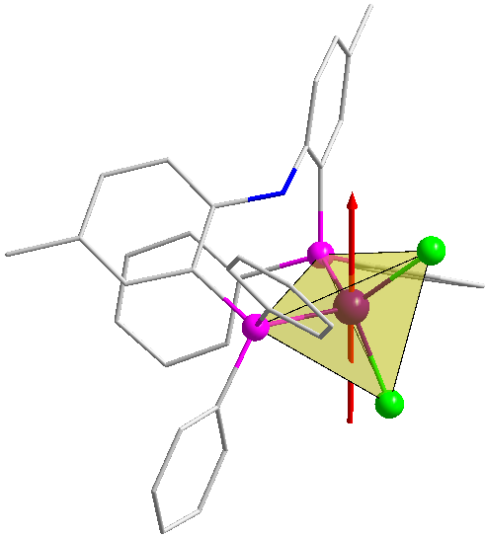

Figure S13. Orientation of the main axis of the *g* tensor for the ground state KD of complex **1**.

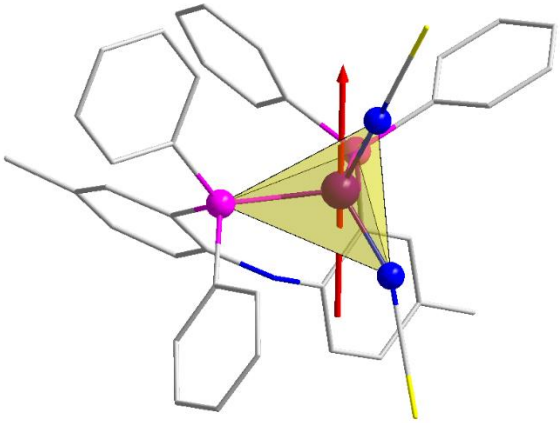

Figure S14. Orientation of the main axis of the *g* tensor for the ground state KD of complex **2**.

References

(1) J. J. Davidson, J. C. DeMott, C. Douvris, *Inorg. Chem*., 2015, **54**, 2916-2935.

(2) *SHELXTL 6.10*, Bruker Analytical Instrumentation, Madison, Wisconsin, USA, 2000.

(3) (a) S. -L. Wang, L. Li, Z. -W. Ouyang, Z. -C. Xia, N. -M. Xia, T. Peng and K. -B. Zhang, *Acta Phys. Sin.*, 2012, **61**, 107601; (b) H. Nojiri, Z. -W. Ouyang, *Terahertz Sci. Technol.*, 2012, **5**, 1.

(4) (a) F. Neese, I. Wiley, *Rev. Comput. Mol. Sci*., 2012, **2**, 73; (b) F. Neese, F. Wennmohs, ORCA (v. 3.0.3), An *ab initio*, DFT and semiempirical SCF-MO package, Max- Planck-Institute for Chemical Energy Conversion, *Stiftstr*., 34-36, 45470 Mulheim a. d. Ruhr, Germany, 2013. (c) F. Neese. *WIREs Comput Mol Sci* 2018, **8**:el1327, doi: 10.1002/wcms.1327.

(5) (a) F. Weigend, R. Ahlrichs, *Phys. Chem. Chem. Phys*., 2005, **7**, 3297; (b) A. Schafer, C. Huber, R. Ahlrichs, *J. Chem. Phys*., 1994, **100**, 5829.

(6) B. A. Hess, *Phys. Rev. A: At., Mol., Opt. Phys*., 1986, **33**, 3742−8.

(7) (a) P. E. M. Siegbahn, J. Almlof, A. Heiberg and B. O. Roos, *J. Chem. Phys.*, 1981, **74**, 2384−2396; (b) C. Angeli, R. Cimiraglia, S. Evangelisti, T. Leininger and J.-P. Malrieu, *J. Chem. Phys.*, 2001, **114**, 10252−10264; (c) C. Angeli, R. Cimiraglia, J.-P. Malrieu, *Chem. Phys. Lett.*, 2001, **350**, 297−305; (d) C. Angeli, R. Cimiraglia,

Theor. Chem. Acc., 2002, **107**, 313−317; (e) C. Angeli, R. Cimiraglia and J.P. Malrieu, *J. Chem. Phys.*, 2002, **117**, 9138−9153.

(8) (a) R. Ruamps, L. J. Batchelor, R. Guillot, G. Zakhia, A. Barra, W. Wernsdorfer, N. Guihéry and T. Mallah, *Chem. Sci.*, 2014, **5**, 3418–3424; (b) R. Ruamps, L. J. Batchelor, R. Maurice, N. Gogoi, P. Jimenez-Lozano, N. Guihery, C de Graaf, A. Barra, J. Sutter and T. Mallah, *Chem. -Eur. J.*, 2013, **19**, 950-956.

(9) (a) A. Abragam and B. Bleaney, *Electron Paramagnetic Resonance of Transition Ions*, Clarendon Press: Oxford, 1970; (b) L. F. Chibotaru and L. Ungur, *J. Chem. Phys.*, 2012, **137**, 064112; (c) L. F. Chibotaru, *Adv. Chem. Phys*., 2013, **153**, 397; (d) L. F. Chibotaru, *Struc. Bond*., 2015, **164**, 185.

(10) F. Neese, *J. Chem. Phys*., 2005, **122**, 034107.

(11) R. M. Maurice, R. Bastardis, C. D. Graaf, N. Suaud, T. Mallah and N. Guihéry, *J. Chem. Theory. Comput*., 2009, **5**, 2977-2984.